High-temperature corrosion fatigue of a ferritic ductile cast iron in inert and corrosive environments at 700°C

M. Ekström[1*], S. Jonsson[1]

[1] Division of Mechanical Metallurgy, Materials Science and Engineering, Royal Institute of Technology, SE-100 44, Stockholm, Sweden

In the present work, low-cycle fatigue testing of a ferritic ductile cast iron named SiMo51 has been carried out in three atmospheres: argon, air and a synthetic diesel exhaust-gas at 700°C. The fatigue life was reduced up to 80% in the worst case. Two crack growth mechanisms were observed and directly linked to oxidation. At weak oxidation, a nodule-to-nodule crack growth occurred. At strong oxidation, crack growth occurred through oxidized material in front of the crack tip.

Keywords: high-temperature LCF, corrosion fatigue, ductile cast iron, crack growth mechanisms

Introduction

The ductile cast iron SiMo51 is used for exhaust manifolds in heavy-duty diesel engines. During operation of the engine, these components are exposed to fatigue, induced by thermal cycling and vibrations, creep and corrosion. Despite this complex environment, data from low-cycle fatigue testing in air is generally used for design calculations of exhaust manifolds. The aim of this study is to determine the reduction in the high-temperature low-cycle fatigue life of SiMo51 at 700°C in air and diesel exhaust gas compared to an inert environment ($Ar+1\%H_2$). In addition, the crack growth mechanisms are examined.

Due to the complexity and high costs of these types of experiments, the results reported on this subject are rather scarce. Most studies concerns Ni-base alloys intended for use in aerospace- and nuclear applications. Experiments have been conducted at high temperatures in, for example, oxygen-containing atmospheres[1,2,3], sulfidizing environments[4,5], carburizing environments[6], jet engine fuel exhausts[7] and in other corrosive gases[8], all showing an increased crack growth rate compared to testing in inert environments. The reduced performance of Ni-base alloys is generally associated with intergranular crack growth, accelerated by diffusion of, for example, oxygen or sulfur, into the grain boundaries in front of the crack tip. For cast irons, no literature was found. As a result, we consider this work to be pioneering.

The microstructure of a ductile cast iron is completely different compared to a Ni-base alloy. SiMo51 consists of a soft ferritic matrix with a distribution of large graphite nodules, which may function as crack initiation points. Ni-base alloys, on the other hand, contain very fine gamma prime precipitates in a high-strength austenitic matrix having a large precipitation hardening and high creep resistance at high temperature. In addition, Ni-base alloys generally contain Cr and Al giving a high-temperature corrosion resistance far more superior than for cast irons. Hence, the high-temperature corrosion fatigue behavior of SiMo51 is expected to be different compared to reported results for Ni-base alloys.

Experimental Procedure

The chemical composition of SiMo51 is Fe-3.17C-4.15Si-0.40Mn-0.10Cr-0.04Ni-0.86Mo-0.052Mg according to chemical analysis. The mechanical properties are given in Table 1 at room temperature and 700°C.

Table 1: E-modulus (E), yield strength (σ_y) and ultimate tensile strength (σ_{UTS}) of SiMo51[9]

T	E (GPa)	σ_y (MPa)	σ_{UTS} (MPa)
RT	159	473	583
700°C	150	42	44

The high-temperature corrosion fatigue tests were conducted at 700°C in three atmospheres: i) Ar+1%H_2, ii) air and iii) synthetic diesel exhaust gas composed of 5%O_2-10%CO_2-5%H_2O-1ppm SO_2-N_2 bal. A mechanical testing machine (Instron 8561) with a set-up as shown in Fig. 1 was used. Dry gas was supplied with an evaporation module for H_2O addition through a heated system (80°C). A quartz tube was fixed between two ceramic plates with machined grooves and rubber seals. Gas-tight seals were applied between the ceramic plates and the test specimen (∅ 7mm), which was heated by an induction coil surrounding the whole setup. An oxygen sensor (Zirox, model SS27) on the outgoing gas was used to ascertain a gas-tight system. A thermocouple of type S was tied to the middle of the gauge length using a heat-resistant thread (Al_2O_3-SiO_2). A laser speckle extensometer was used for strain measurement locking speckle patterns (9mm apart) on the test specimen between the induction coil windings. The tests were performed symmetrically (R= -1) with a constant cycling time of 30s per cycle (0,03Hz). For each environment, 6 to 8 strain amplitudes were applied, generating a lifetime of 300 to 30,000 cycles. A 90% tensile load drop was used as fracture criteria triggering a simultaneous shutdown of heating and gas supply.

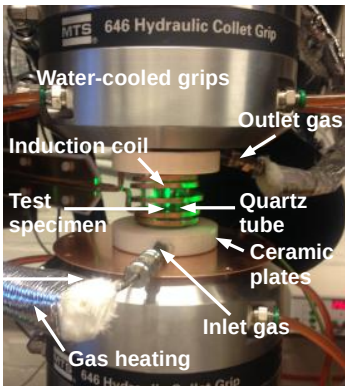

Fig. 1: Illustration of experimental setup.

Results and discussion

LCF life

The results from the LCF tests are presented in Fig. 2a as ε-N_f curves. As expected, the fatigue life is lower in the corrosive environments, i.e. in air and in diesel exhaust gas, compared to the inert argon environment. It is observed that the fatigue life in the exhaust gas is approx. 30-50% lower than in air and approx. 60 to 75% lower than in the inert environment, see Fig. 2b. Moreover, it is noted that the fatigue life in air is approx. 15 to 65% lower than in argon, with the highest reduction observed at the lowest strain amplitudes, where the interaction between the environment and the crack is the highest. The tests were stopped at 30,000 cycles and specimens reaching this limit were indicated as run outs.

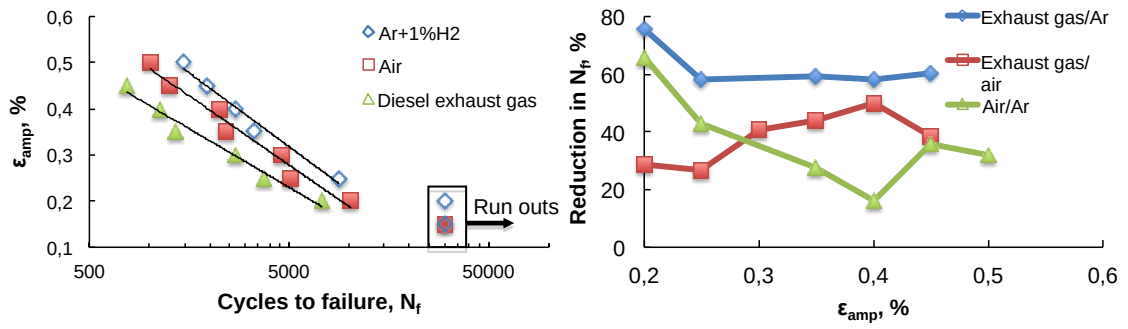

(a) (b)

Fig. 2: LCF data for SiMo51 at 700°C in Ar+1%H_2, air and diesel exhaust gas showing **a)** ε-N_f-plot and **b)** reduction in fatigue life.

Fracture behavior

As shown in Figs. 3a-c, the crack growth in all environments mainly showed a one-directional crack growth with initiation at the surface of the test specimen. The subsequent crack growth behavior was, however, different. During testing in Ar+1%H_2, the cracks were observed to grow from one graphite nodule to another revealing a high amount of graphite nodules in the crack growth zone on the fracture surface. In a higher magnification, cracking in the ferritic matrix was also observed. The fracture zone showed significantly lower graphite content suggesting a rupture through the ferrite. All specimens tested in the argon environment showed an oxide rim (approx. 500-1000µm wide) in the initiation zone indicating presence of oxygen in the beginning of the crack growth. See Fig. 4.

During testing in air, the complete crack growth zones were oxidized (Fig. 5b). Generally, two types of crack growth behaviors were observed. The first and most commonly observed type is crack growth combined with oxidation reactions. Fig. 5c and 5d shows an example of such crack growth. The oxide scale formed on the metal surface is fairly thick, approx. 40µm, suggesting a slow crack growth rate allowing for oxidation reactions to occur. The other type of crack growth observed is a nodule-to-nodule growth, as seen for the argon environment. These cracks are long and contain a low amount of oxides (see Fig. 5e), suggesting a fast crack growth rate. The number of secondary cracks was found to be higher in air compared to in Ar+1%H_2. As illustrated in Fig. 5f, small cracks growing close to each other may cause failure if the cracks meet. The final fracture zone showed similar appearance as in Ar+1%H_2 (Fig. 5a) with rupture occurring mainly in the ferritic phase.

During testing in diesel exhaust gases, the fracture surface showed similar appearance as in air with a completely oxidized crack growth zone, see Fig. 6a. As seen in air, LCF in diesel exhaust gas also resulted in two different crack growth behaviors. A few regions showed nodule-to-nodule growth but the dominating type was the combination of crack growth and oxidation. For the dominating growth type, thick oxide scales are formed in front of the crack tip, which is illustrated in Figs. 6c-f. In Figs. 6e and 6f it can be seen that a crack extends through the oxide scale suggesting that the material in front of the crack tip is oxidized followed by crack growth through the oxide scale.

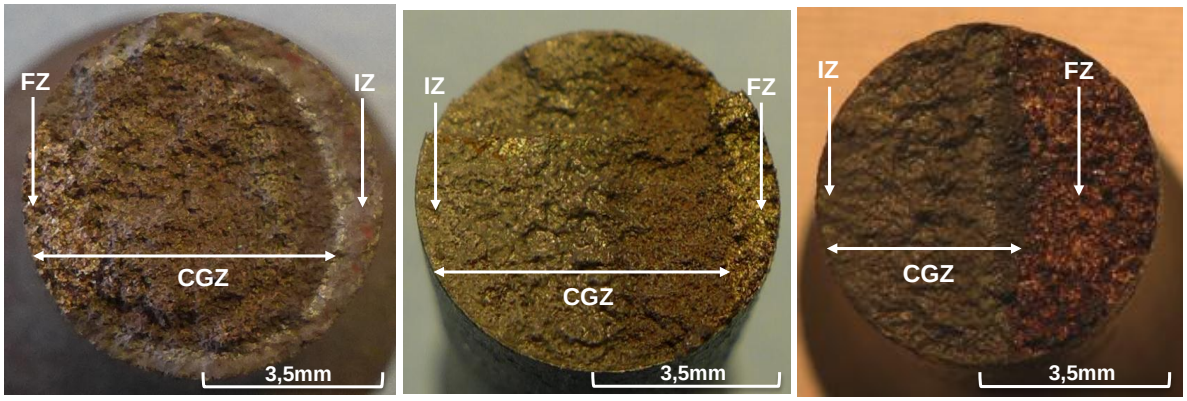

(a) (b) (c)

Fig. 3: Images showing initiation zone (IZ), crack growth zone (CGZ) and fracture zone (FZ) on the fracture surfaces of SiMo51 tested with LCF at 700°C in **a)** Ar+1%H_2 (ε_{amp} 0.25%), **b)** air (ε_{amp} 0.25%) and **c)** diesel exhaust gas (ε_{amp} 0.20%).

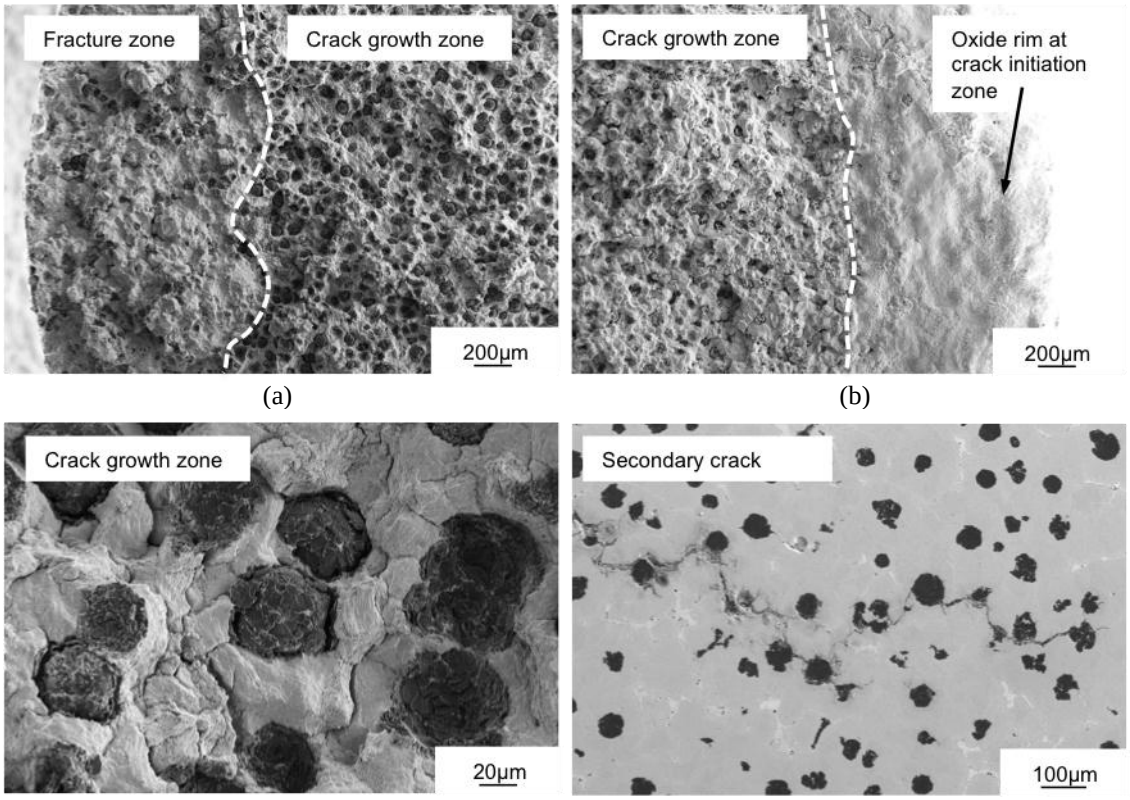

Fig. 4: SEM images of SiMo51 tested in Ar+1%H_2 (ε_{amp} 0.25%) showing **a)** CGZ and FZ, **b)** IZ and CGZ, **c)** CGZ in higher magnification and **d)** growth of a secondary crack.

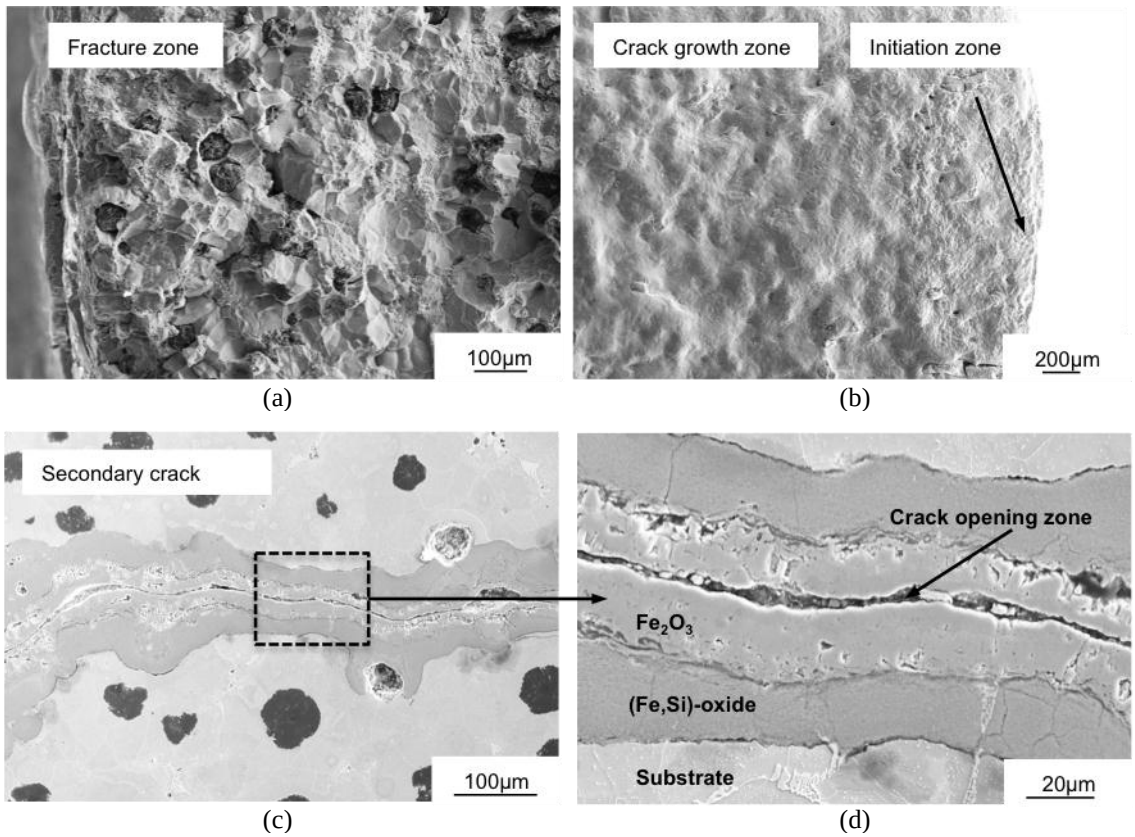

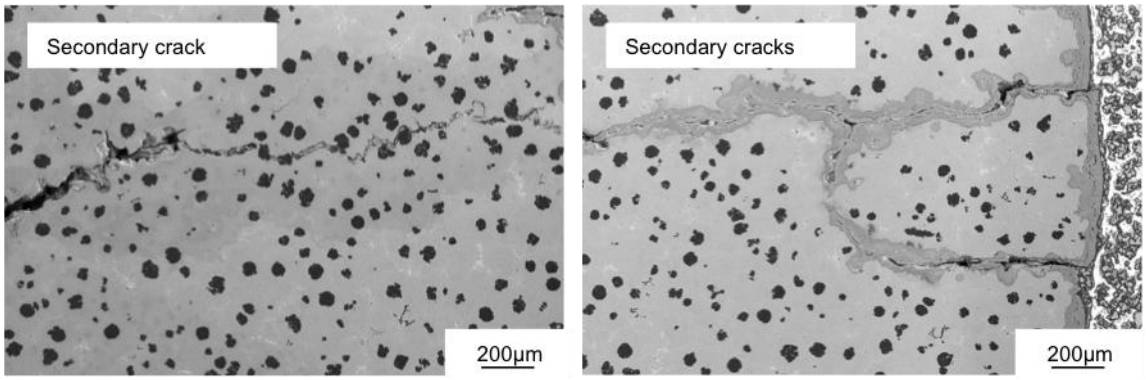

(e) (f)

Fig. 5: SEM images of SiMo51 tested in air (ε_{amp} 0.25%) showing **a)** FZ **b)** IZ and CGZ, **c)** secondary crack, **d)** secondary crack in higher magnification, **e)** secondary crack and **f)** two secondary cracks.

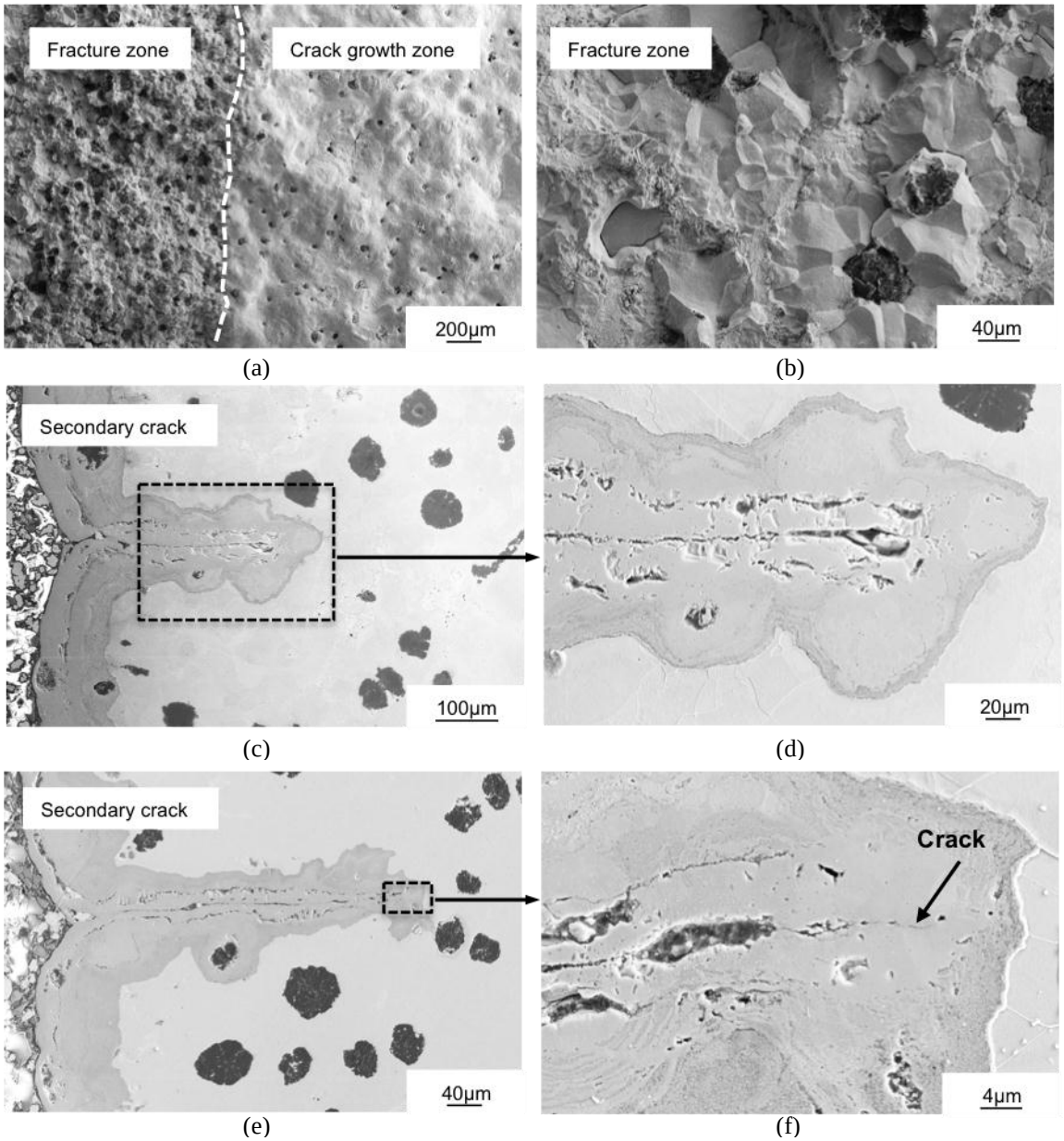

(a) (b)

(c) (d)

(e) (f)

Fig. 6: SEM images of SiMo51 tested in diesel exhaust gas (ε_{amp} 0,2%) showing **a)** FZ and CGZ **b)** FZ, **c)** secondary crack, **d)** c in higher magnification, **e)** secondary crack (ε_{amp} 0.3%) and **f)** e in higher magnification.

Characterization of oxide phases

XRD on fracture surfaces and EDX on cross-sections were applied for characterization of the oxide scale formed during LCF. A compilation of the results is found in Table 2. The fracture surface in argon generally showed no oxide, except of an oxide rim formed in the initiation zone at the beginning of the crack growth. This oxide rim showed a double-layer structure (approx. 80μm thick) with an outer layer of Fe_2O_3 and an inner layer of (Fe, Si)-oxide (phase not characterized). Testing in air resulted in oxide formation in the whole crack growth zone, showing a scale structure of outer Fe_2O_3 and inner (Fe, Si)-oxide. In exhaust gas, the crack growth zones were also completely oxidized forming a double-layer structure. In this environment, Fe_2O_3 and FeOOH were detected in the outer layer and (Fe, Si)-oxide in the inner layer. None of the examined samples showed formation of a compact SiO_2 barrier layer at the metal/oxide interface, which has been observed during oxidation testing of non-loaded specimens in air[10].

Table 2: Phases formed on fracture surfaces.

Ar+1%H_2	**Air**	**Diesel exhaust gas**
Bcc	Fe_2O_3	FeOOH
Fe_2O_3	(Fe,Si)-oxide	Fe_2O_3
(Fe,Si)-oxide		(Fe,Si)-oxide

Conclusions

In the present study, high-temperature corrosion fatigue has been studied for the cast ductile iron SiMo51 at 700°C in three atmospheres: Ar+1%H_2, air and synthetic diesel exhaust gas. The following was concluded:

1. Testing in air and in diesel exhaust gas results in a reduction of the LCF life of SiMo51 and is linked to oxidation interaction between the metal and the environment.
2. The fatigue life reduction for (diesel exhaust gas)/(Ar), (diesel exhaust gas)/(air) and (air)/(Ar) is approx. 60-75%, 30-50% and 15-65%, respectively.
3. Two crack growth mechanisms were observed. The first, showing low or no influence of oxidation, was characterized as a nodule-to-nodule crack growth. It was observed in inert environments and during fast crack growth, where there is little time for oxidation reactions. The second mechanism shows a strong influence from oxidation and is characterized by oxidation in front of the crack tip followed by crack growth in the oxide.
4. The oxide scales formed in air showed a double-layer structure consisting of outer Fe_2O_3 and inner (Fe, Si)-oxide. No distinct SiO_2 barrier layer was observed.
5. The oxide scales formed in the diesel exhaust gas showed a double-layer structure consisting of outer Fe_2O_3/FeOOH and inner (Fe, Si)-oxide. No distinct SiO_2 barrier layer was observed.

References

1. R. Molins, G. Hochstetter, J. C. Chassaigne and E. Andrieu: *Acta Mater.*, 1997, 45, 663-674.
2. E. Andrieu, R. Molins, H. Ghonem and A. Pineau: *Mater. Sci. Eng. A*, 1992, 154, 21-28.
3. M. Reger and L. Rémy: *Metall. Trans. A*, 1988, 19, 2259-2268.
4. S. Floreen and R.H. Kane: *Metall. Trans. A*, 1982, 13, 145-152.
5. S. Floreen and R.H. Kane: *Metall. Trans. A*, 1984, 15, 5-10.
6. S. Floreen and C.J. White: *Metall. Trans. A*, 1981, 12, 1973-1979.
7. K.G. Schmitt-Thomas, H. Meisel and H.J. Dorn: *Mater. Corros.*, 1978, 29, 1-9.
8. S. Floreen and R.H. Kane: *Metall. Trans. A*, 1979, 10, 1745- 1751.
9. M. Ekström and S. Jonsson: *Mater. Sci Eng. A*, 2014, 616, 78-87.
10. M. Ekström, P. Szakalos and S. Jonsson: *Oxid. Met.*, 2013, 80, 455-466.

Acknowledgement

This work was done within The Department of Materials Science and Engineering at the Royal Institute of

Technology, KTH, in co-operation with Scania CV. The authors acknowledge VINNOVA for financial support (Grant no. 2012-01690). The authors also thank I. Soroka at the Department of Chemical Science and Engineering, KTH for running the XRD-analysis and the technicians at Materials Technology, Scania CV for support of in sample preparation.